Electronic Supplementary Material (ESI) for Dalton Transactions

Ruthenium Cryptates with an Unusual Selectivity for Nitrate

Naomi A. C. Baker, Nicholas C. Fletcher, Peter N. Horton and Michael B. Hursthouse

Supplementary Data

Table S1: Selected angles and bond lengths [Å and °] for $[Ru(L3)](PF_6)_2$

N5–Ru1	2.050(7)	N9–Ru1–N10	78.7(3)
N6–Ru1	2.057(9)	N9–Ru1–N5	95.4(3)
N7–Ru1	2.053(8)	N10–Ru1–N5	172.2(3)
N8–Ru1	2.079(9)	N9–Ru1–N7	93.1(3)
N9–Ru1	2.021(8)	N10–Ru1–N7	92.4(3)
N10–Ru1	2.032(7)	N5–Ru1–N7	93.1(3)
		N9–Ru1–N6	91.5(3)
		N10–Ru1–N6	96.7(3)
		N5–Ru1–N6	78.1(4)
		N7–Ru1–N6	170.4(3)
		N9–Ru1–N8	170.7(4)
		N10–Ru1–N8	97.9(3)
		N5–Ru1–N8	88.7(3)
		N7–Ru1–N8	78.2(4)
		N6–Ru1–N8	97.5(4)

Table S2: Hydrogen bonds [Å and °] for $[Ru(L3)](PF_6)_2$

D–H···*A*	*d*(*D*–H)	*d*(H···*A*)	*d*(*D*···*A*)	∠(*D*H*A*)
N3–H3···F16	0.88	2.00	2.850(14)	161.9
N3–H3···F113	0.88	2.50	3.14(4)	130.4
N4–H4···O2	0.88	2.11	2.967(12)	163.4

Table S3: Bond lengths [Å] and angles [°] for [Ru(L4)](Br)$_2$.

Ru1-N2	2.033(6)	N2-Ru1-N61	174.0(2)
Ru1-N61	2.046(6)	N61-Ru1-N32	88.4(2)
Ru1-N32	2.049(6)	N2-Ru1-N1	78.8(3)
Ru1-N1	2.061(6)	N61-Ru1-N1	96.4(2)
Ru1-N62	2.061(6)	N32-Ru1-N1	172.9(2)
Ru1-N31	2.063(6)	N2-Ru1-N62	97.9(2)
		N61-Ru1-N62	78.6(2)
		N32-Ru1-N62	94.2(2)
		N1-Ru1-N62	92.0(2)
		N2-Ru1-N31	92.2(2)
		N61-Ru1-N31	91.8(2)
		N32-Ru1-N31	78.6(3)
		N1-Ru1-N31	95.9(2)

Table S4: Hydrogen bonds [Å and °] for [Ru(**L4**)](Br)$_2$.

D–H···*A*	*d*(*D*–H)	*d*(H···*A*)	*d*(*D*···*A*)	∠(*D*H*A*)
N1–H1···O91^{i}	0.883(10)	2.05(5)	2.835(9)	148(7)
N2–H2A···O1^{ii}	0.882(10)	2.08(3)	2.938(9)	166(8)
N31–H31···O92	0.878(10)	2.11(5)	2.882(8)	147(8)
N32–H32···Br2	0.880(10)	2.45(2)	3.318(6)	169(8)
N51–H51···Br2^{iii}	0.880(10)	2.46(4)	3.270(6)	153(7)
N52–H52···Br1	0.878(10)	2.535(14)	3.410(7)	175(8)
O91–H91A···Br1	0.85(3)	2.43(3)	3.275(6)	173(9)
O91–H91B···O51	0.83(3)	1.94(3)	2.758(7)	168(10)
O92–H92A···Br2^{iii}	0.85(3)	2.61(6)	3.402(7)	157(11)
O92–H92B···O52	0.85(3)	2.00(6)	2.796(8)	155(11)
O93–H93A···O32	0.87(3)	1.93(4)	2.777(8)	163(9)
O93–H93B···O1	0.86(3)	2.12(6)	2.895(9)	150(11)

Symmetry transformations used to generate equivalent atoms:
(i) –x,–y+1,–z (ii) –x,–y,–z (iii) –x,–y+1,–z+1

(a)

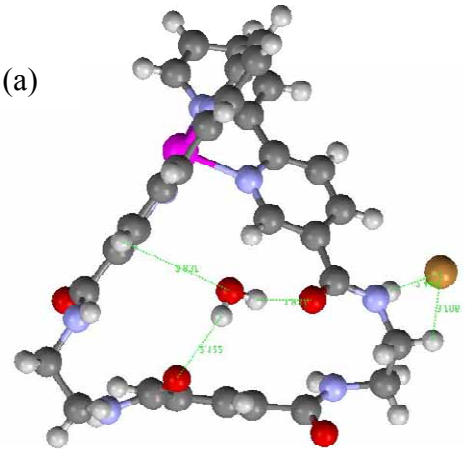

(b)

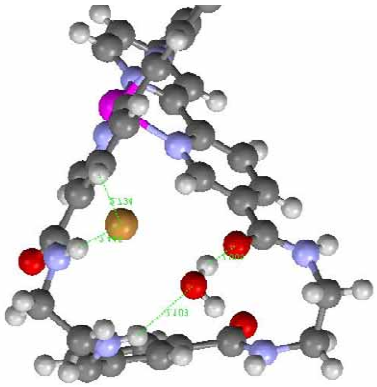

(c)

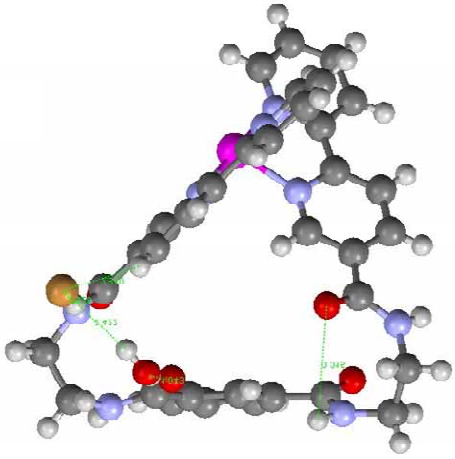

Figure S1a-c: X-ray crystallographic determination of the three cavity faces illustrating the hydrogen bonding networks and location of the bromide anions.

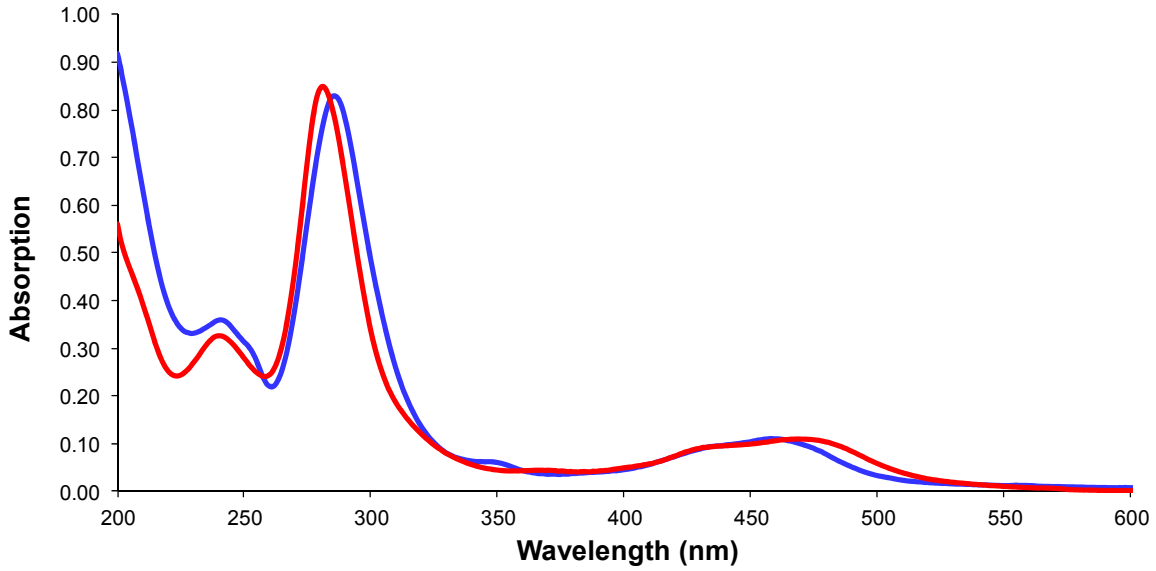

Figure S2a: UV/Vis spectroscopy characterisation of $[Ru(L3)](PF_6)_2$ (red) and $[Ru(L4)](PF_6)_2$ (blue) in CH_3CN with respective concentrations of 1.55 $x10^{-5}$ M and $1.43x10^{-5}$ M respectively at room temperature.

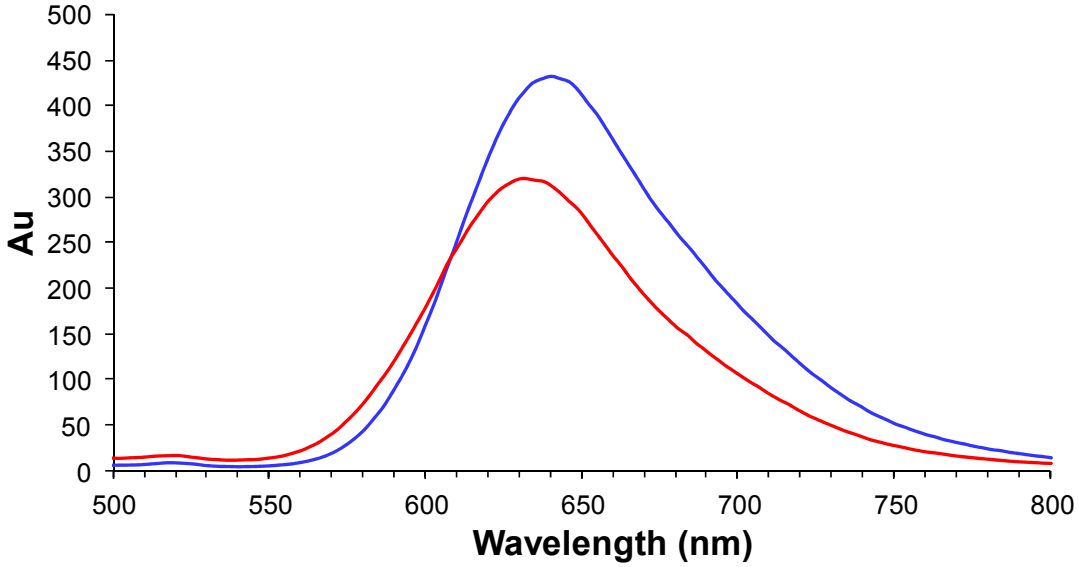

Figure S2b: : Luminescence characterisation of $[Ru(L3)](PF_6)_2$ (red) and $[Ru(L4)](PF_6)_2$ (blue) in CH_3CN at room temperature excited at 450 nm with an absorption of 0.1.

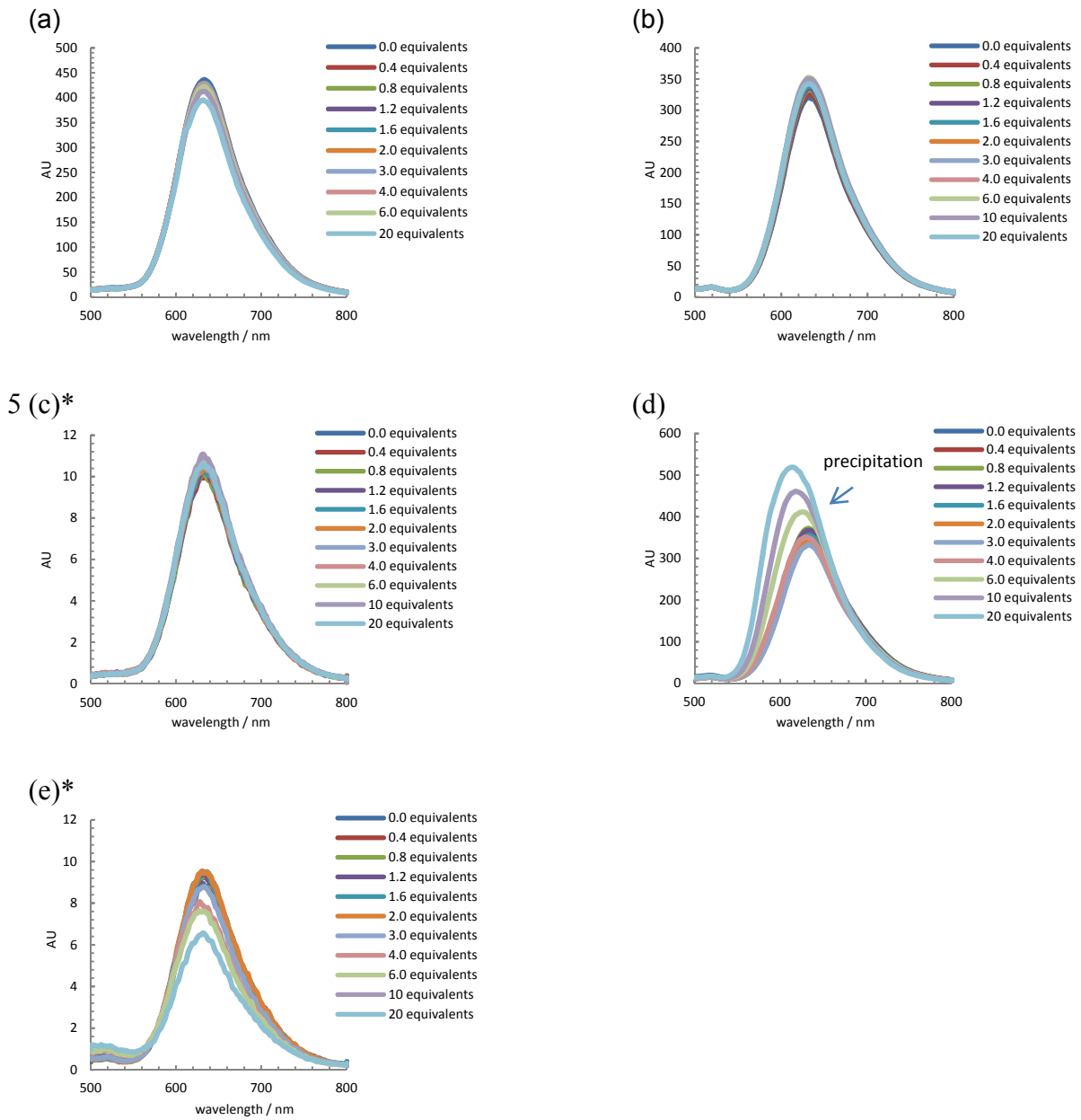

Figure S3: Luminescence characterisation of $[Ru(L3)](PF_6)_2$ on the sequential addition of tetrabutylammonium **(a)** chloride, **(b)** bromide, **(c)** nitrate, **(d)** hydrogensulfate and (e) dihydrogenphosphate (approx. 5×10^{-6} M, CH_3CN, 25 ºC, excited at 450 nm).

* Spectrum run at reduced detection slit widths to avoid saturation of the detector.

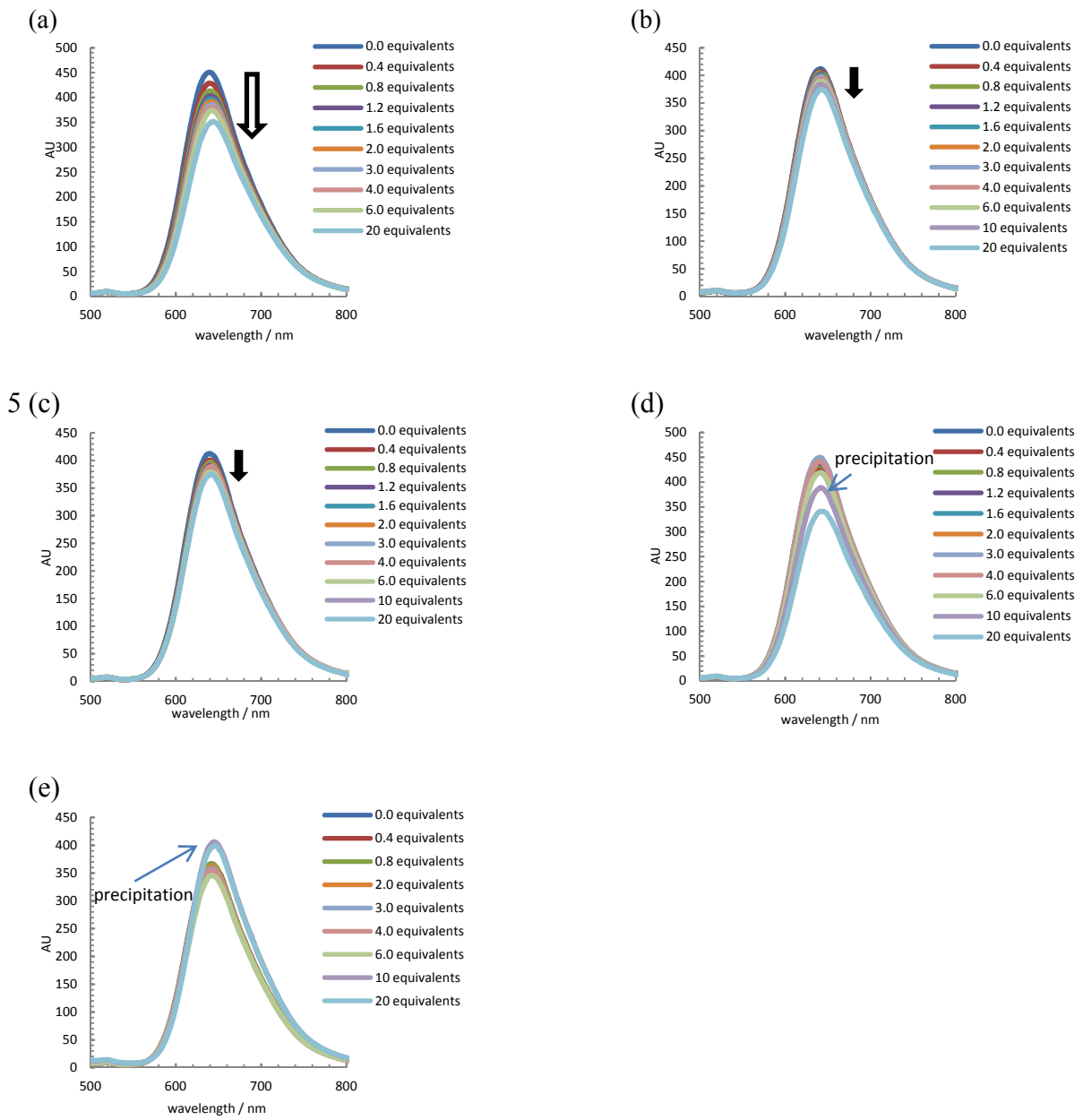

Figure S4: Luminescence characterisation of $[Ru(L4)](PF_6)_2$ on the sequential addition of tetrabutylammonium **(a)** chloride, **(b)** bromide, **(c)** nitrate, **(d)** hydrogensulfate and (e) dihydrogenphosphate (approx. 5×10^{-6} M, CH_3CN, 25 ºC, excited at 450 nm).

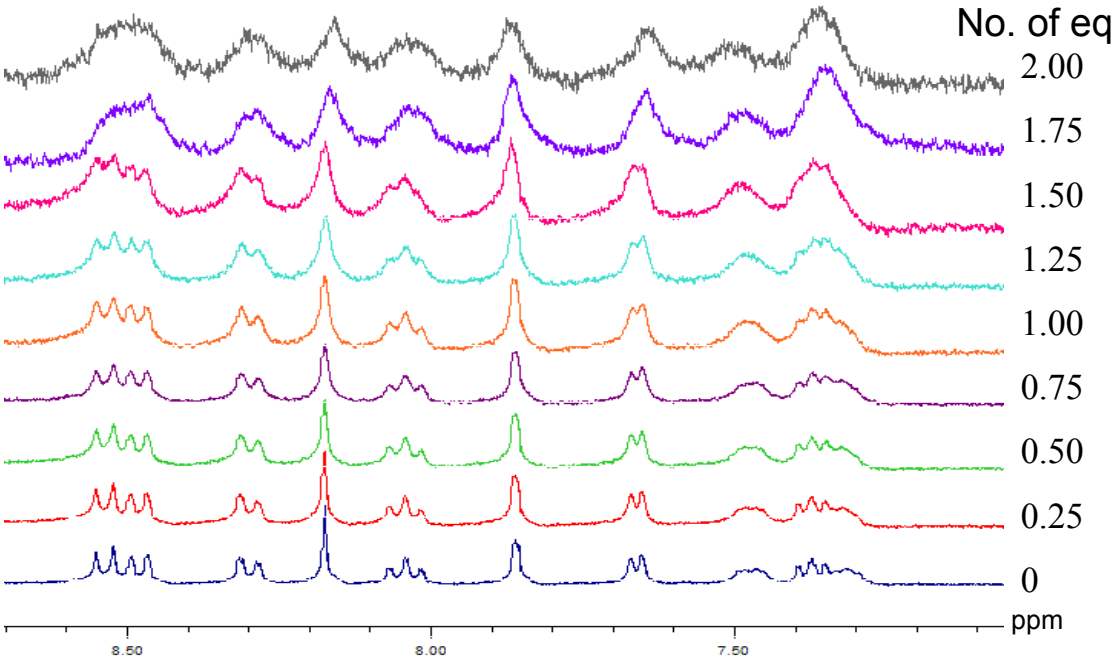

Figure S5: ^{1}H NMR spectroscopic titration of $NEt_4H_2PO_4$ with $[Ru(L4)](PF_6)_2$ (300 MHz, CD_3CN, initial metal complex concentration 5×10^{-4} M at 25 C) - similar loss of resolution observed with $[Ru(L3)](PF_6)_2$ (not shown) along with observed precipitation.

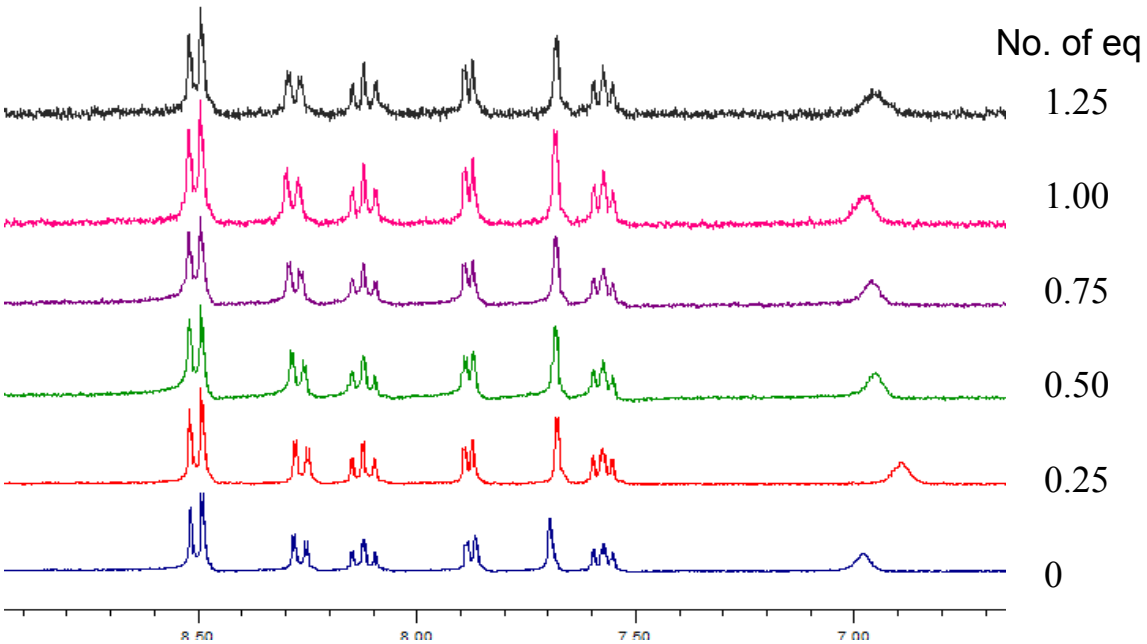

Figure S6: ^{1}H NMR spectroscopic titration of NEt_4HSO_4 with $[Ru(L3)](PF_6)_2$ (300 MHz, CD_3CN, initial metal complex concentration 5×10^{-4} M at 25 C) - similar spectrum observed with complex $[Ru(L4)](PF_6)_2$ (not shown).

(a)

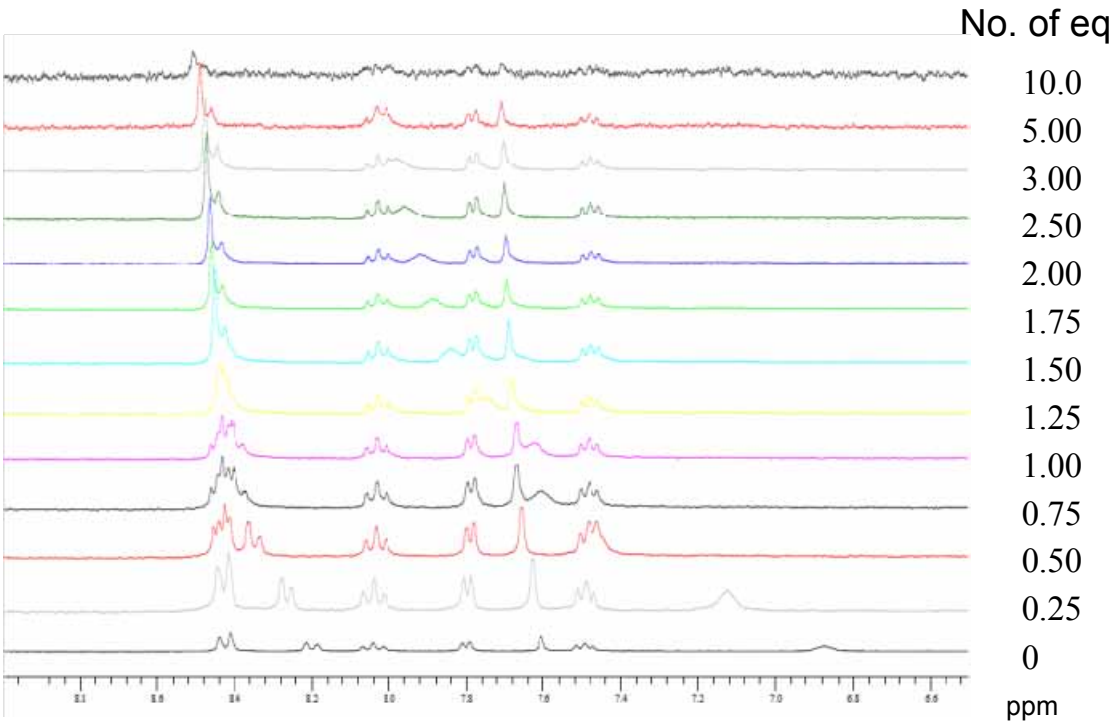

(b)

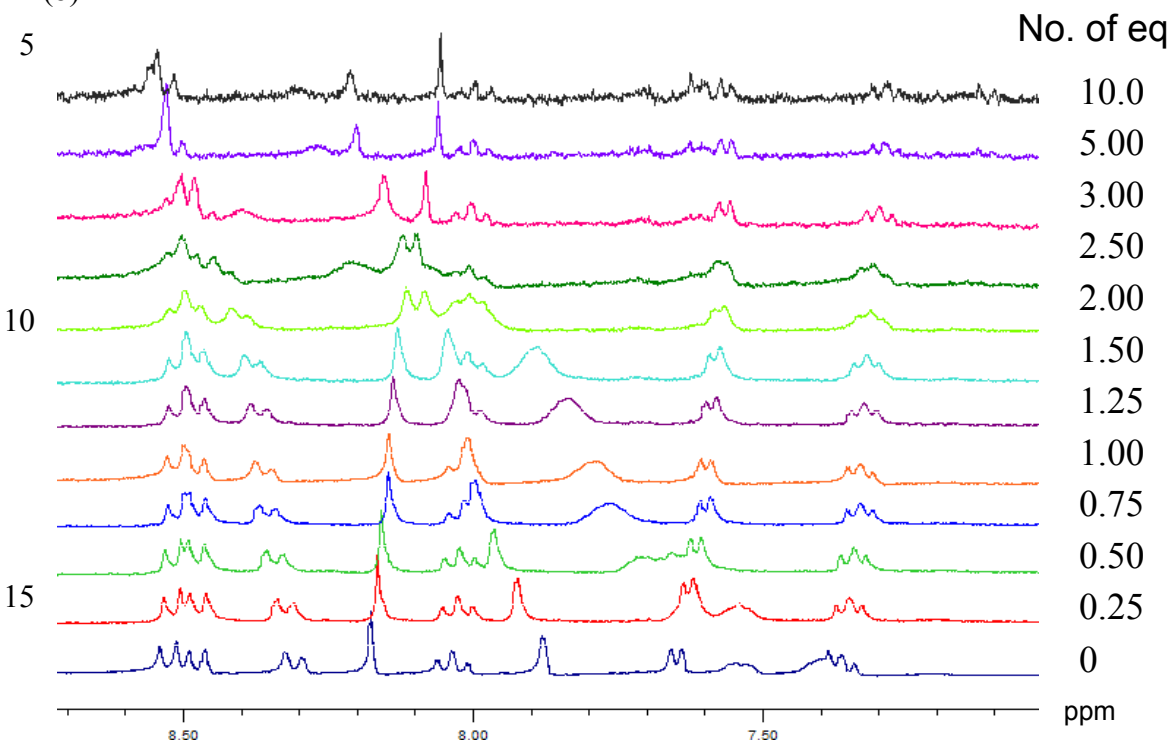

Figure S7: ^{1}H NMR spectroscopic titration of NEt_4Cl with (a) $[Ru(L3)](PF_6)_2$ and (b) $[Ru(L4)](PF_6)_2$ 20 (300 MHz, CD_3CN, initial metal complex concentration 5×10^{-4} M at 25 C)

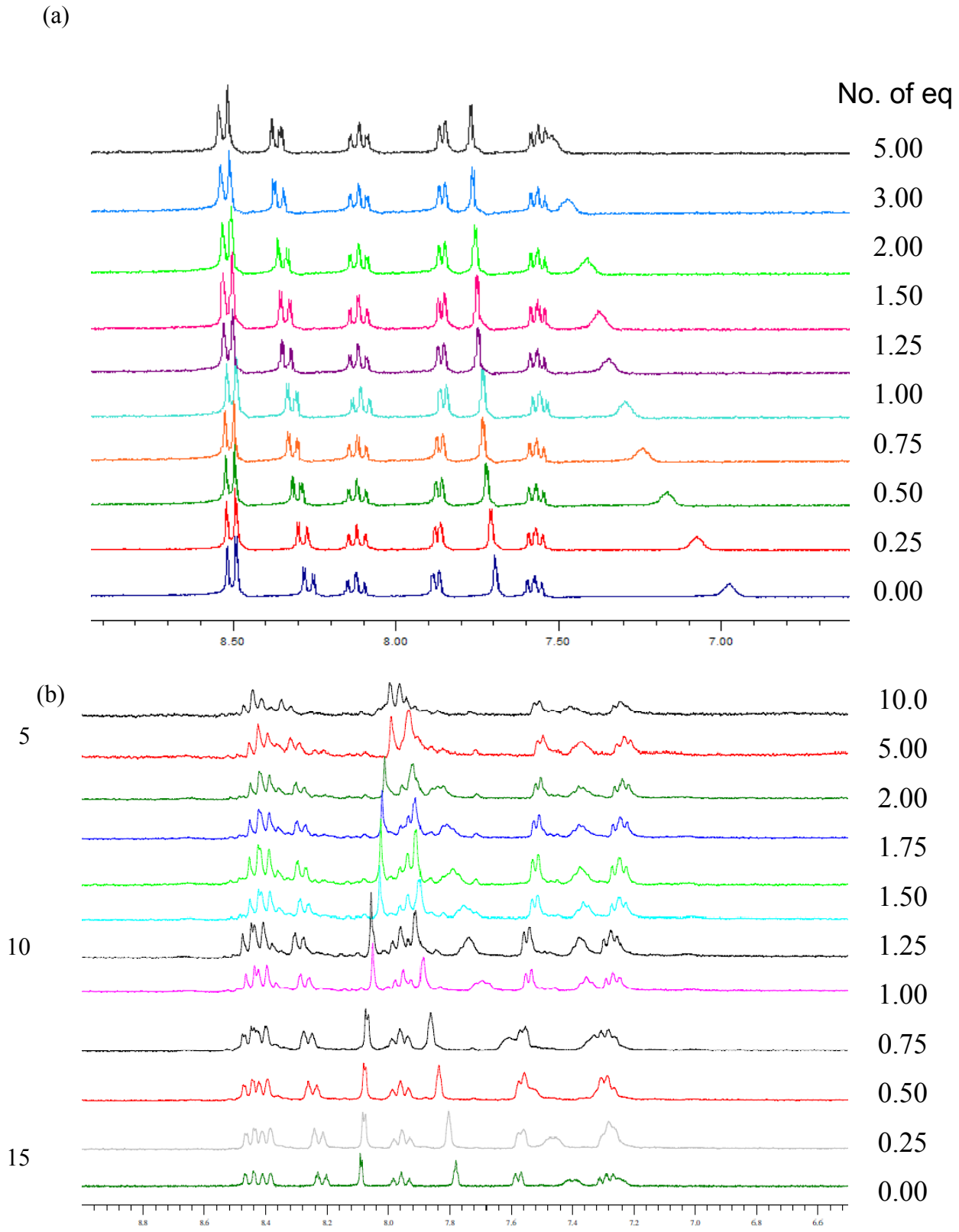

Figure S8: ^{1}H NMR spectroscopic titration of NEt_4NO_3 with (a) $[Ru(L3)](PF_6)_2$ and (b) $[Ru(L4)](PF_6)_2$ (300 MHz, CD_3CN, initial metal complex concentration 5×10^{-4} M at 25 C)

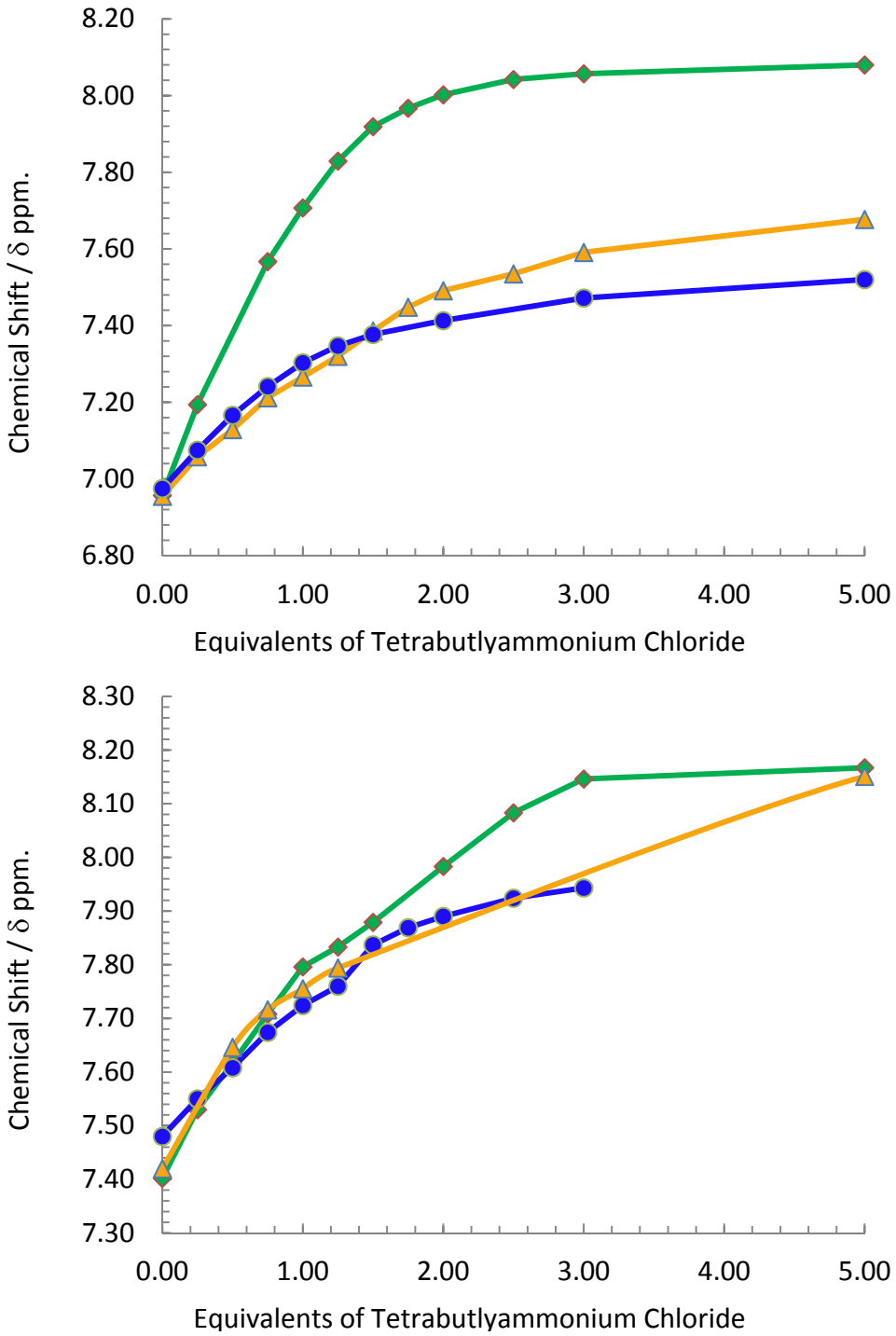

Figure S9: ^{1}H-NMR spectroscopy titration showing the movement of the principle amide peak of (a) [Ru(L3)]$(PF_6)_2$ and (b) [Ru(L4)]$(PF_6)_2$, on the sequential addition of tetrabutylammonium ions. (NB stability constants were calculated for a range of protons, not just the highlighted amides – the data for the amide shift observed with the addition of TBABr to [Ru(L4)]$(PF_6)_2$ was not used in the determination of stability constants due to inadequate data arising from overlapping peaks).